Pergamon

Int. J. Multiphase Flow Vol. 22, No. 5, pp. 969–989, 1996

0301-9322/96 $15.00 + 0.00

PII: S0301-9322(96)00017-1

SLOW FLOW THROUGH A MODEL FIBROUS POROUS MEDIUM

A. M. J. DAVIS[1] and D. F. JAMES[2]

[1]Department of Mathematics, University of Alabama, Tuscaloosa, AL 35487-0350, U.S.A.
[2]Department of Mechanical Engineering, University of Toronto, Toronto, Canada, M5S 1A4

(Received 11 July 1995; in revised form 27 February 1996)

Abstract—Analytical techniques are used to find the permeability of a model of a fibrous porous medium. The model is an array of thin annular disks periodically spaced in planes normal to the flow, where the repeating unit is a square or an equilateral triangle, and the planes are uniformly spaced in the flow direction. The solution of the Stokes equations for flow through the array is found by the method of distributed singularities, and the drag on a disk is estimated by an asymptotic technique in which the ratio of the radii of each annulus tends to unity. From the drag, the flow resistance or permeability of the array is found. By matching the thin disks to thin rings (tori), the array simulates fibrous materials like filters, in which the fibers are curved, perpendicular to the flow, and randomly oriented. Calculations of permeability are made for various ring sizes and spacings, for three array configurations, and for solid volume fractions in the range 0.0002–0.02. The results show that minimum permeability generally occurs for the most uniform distribution of solid material in a plane. Comparisons with equivalent rod arrays reveal that ring arrays generally have higher permeabilities, even though the rings create more tortuous flow paths. Copyright © 1996 Elsevier Science Ltd

Key Words: Stokes flow, model, fibrous, porous medium

1. INTRODUCTION

Porous materials made of fibers have a much wider range in flow resistance than porous media made of granular particles because the porosity range is much greater. Granular materials are necessarily compact and consequently have porosities around 35%. Fibrous materials, on the other hand, are generally uncompressed and the porosity can be as high as 99%. The range in porosity is more evident when stated in terms of the volume fraction of solid material, ϕ, because ϕ ranges from 0.01 to 0.5 for fibrous materials. A common such material is a filter, which is normally used to sieve particles of a particular size. Given the particle size and fiber diameter, one can straightforwardly determine how much material is required for a filter, or what ϕ must be, assuming a uniform spacing of fibers. Not so easily determined is the permeability or flow resistance, which is usually required when designing a flow system which includes the filter. Estimates of permeability can be made from related experimental data or from theoretical formulas. In theoretical work, the medium is usually modelled as an array of straight, parallel rods oriented normal to the flow. In materials like filters, the fibers are normal to the flow but they are usually curved and randomly oriented. The geometrical complexity can be seen in pictures of fibrous materials. Curvature is evident, for example, in photographs of kraft pulp (Bolam 1962), steel wool (Battista 1964), and New Zealand flax (Isenberg 1967), which show that the curvature is variable and that the radius of curvature is of order ten times the fiber diameter. Curvature is also a feature in macromolecular filters, which are aqueous solutions of long-chain polymers. These filters occur in natural and man-made processing systems to inhibit or prevent the transport of colloidal particles, and the polymer chains are randomly-coiled and intertwined. A distinguishing feature of macromolecular filters is that the solidities are very low: ϕ is typically of order 0.0001 (Ogston *et al.* 1973), much lower than the minimum of 0.01 for normal, macroscopic filters (Jackson & James 1986).

The geometrical feature which most influences permeability is the uniformity of fiber spacing, and studies have attempted to quantify the relationship between permeability and uniformity. Yu & Soong (1975) investigated the relationship by developing a model to estimate the flow resistance for parallel, randomly-distributed rods. They found that the permeability could be as much as 50%

above the minimum, i.e. above the permeability for uniform spacing throughout. Sangani & Yao (1988) also determined the permeability of random arrays of infinitely long cylinders. They found that, for ϕ between 0.1 and 0.5, the variation in permeability over several random configurations was small. This finding differs somewhat from that of Yu and Soong, but the latter's method was approximate and ϕ was an order of magnitude smaller. Howells (1974) attempted to study the effect of randomness by considering the drag exerted on a sparse array of small fixed spheres or parallel circular cylinders. His leading approximation is the Brinkman model, in which the effect on one object of all the others is treated as a Darcy resistance, thus introducing the concept of an effective medium. The higher approximations take into account modifications in the mean flow due to pairwise interactions between the spheres or cylinders, but the work does not reveal the difference in flow resistance between ordered and random arrays.

To our knowledge, the only experiment dealing with uniformity was the one carried out by Kirsch & Fuchs (1967). They measured the flow resistance of parallel rods arranged in various ways and found permeabilities up to 100% larger for non-uniform arrays than for uniform arrays. Even wider variations in permeability have been obtained for actual fibrous materials, as one might expect. Jackson & James (1986) collected data of flow resistance for a wide variety of porous materials—from glass wool to collagen fibers—and plotted the results as dimensionless permeability versus ϕ. If the fibers in the different materials had had the same configuration, the data should have collapsed on to a single curve. However the plot shows a three-fold variation in dimensionless permeability for a fixed value of ϕ. Some of this variation is due to fiber curvature and orientation, but the greatest part is likely due to the non-uniform spacing.

As mentioned above, the prior theoretical works have generally modelled the medium as an array of parallel rods, aligned either perpendicular or parallel to the flow. The array configuration which has received the most attention is the periodic square array because the spacing is uniform and the mathematics is simpler than for any other configuration. Analytical solutions for Stokes flow through a square array have been obtained by Hasimoto (1959), Sangani & Acrivos (1982) and Drummond & Tahir (1984). Their analytical techniques differ but, for rods perpendicular to the flow, which is the case relevant to the present work, they yield the same equation:

$$\frac{k}{a^2} = \frac{1}{8\phi}\left[\ln\left(\frac{1}{\phi}\right) - 1.476 + 2\phi + \mathrm{O}(\phi^2)\right], \qquad [1]$$

where k is the permeability in Darcy's Law and a is the rod radius. Sangani & Acrivos found that the corresponding equation for a hexagonal array is almost the same as the above equation, the constant being 1.490 instead of 1.476.

A regular arrangement of straight parallel rods is convenient for solving the Stokes equations, but such arrays do not adequately represent the complex, three-dimensional structures in fibrous materials. We sought to create an alternate model, one which more closely simulates the actual geometry but still allows an analytic solution of the Stokes equations. We particularly wanted to incorporate fibers which are curved and therefore variably oriented because these geometrical features have not been part of any prior study. We also wanted the model to allow variable fiber spacing, so that we would be able to explore the influence of uniformity on flow resistance. A model which has these features is a periodic array of thin tori or rings, aligned normal to the flow. The rings create curvature *per se*, and the arcs have various orientations. The flow in a ring array is inherently three-dimensional, and thus this type of array is more realistic than the two-dimensional flow in rod arrays. The spacing between rings can be varied in the model and thus it will be possible to explore how permeability is affected by material distribution.

1.1. Ring model

The unit structure of our fibrous medium is a periodic arrangement of identical thin rings in a plane. One such arrangement, with the square as the repeating unit, is sketched in figure 1. The three-dimensional array is an open stack of such planes, equally spaced and normal to the flow. Two arrays with this unit structure are considered here. In one, the planes are arranged such that the rings are aligned, i.e. they lie one behind the other. In the other, alternate planes are offset to create optimal misalignment; the alternate planes are shifted laterally such that the centers of rings alternate with the centers of squares. In this latter structure, the solid elements are continually in

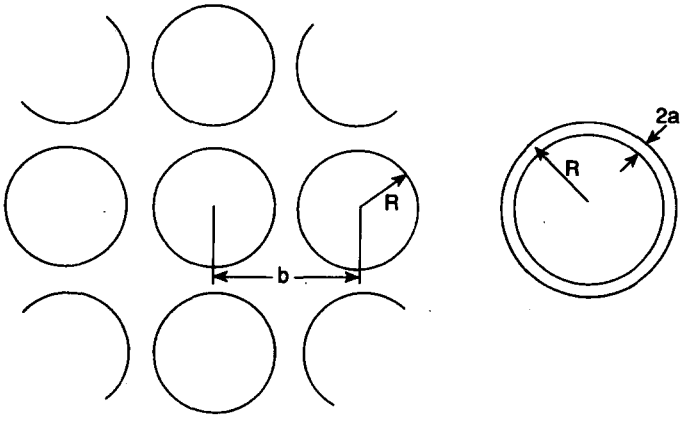

Figure 1. Square arrangement of tori (rings) in a plane. Each torus is defined by radii a and R, with $a \ll R$ so that slender-body theory can be applied.

the path of the flow, and so this array is more representative of fibrous materials. One expects the flow resistance of this "offset" array to be greater, and the present work is undertaken to quantify this effect.

While the thin ring is a natural representation of a curved fiber, the torus is also the only hollow boundary for which Stokes-flow analytical solutions are available. Stewartson (1983) used an analytical solution to show how fluid is reluctant to flow through the torus, a feature which is emphasized here. The slender body theory of Cox (1970), reviewed by Lighthill (1976), used the flow past a straight circular cylinder for the inner field of flow past a curved body; hence he did not take account of local center-line curvature. Johnson & Wu (1979) applied slender body theory to various motions of a torus without making the above approximation; they effectively summed the series in powers of $(\ln \epsilon)^{-1}$, the terms which arise in Cox' method, to obtain the force with errors of order ϵ^2, where ϵ is the ratio of the cross-sectional radius to the radius of curvature. This analysis could be extended to the periodic arrays considered here and the same results would be obtained, so that slender body theory provides the essential method. However, the calculations for a torus are sufficiently complex that a simpler method is sought. The chosen method is to introduce an equivalent body, the thin annular disk, with dimensions chosen to produce the same drag force, as the torus, to $O(\epsilon)$, for broadside motion in an otherwise unbounded flow. We then take advantage of the known and easier calculation of the force exerted by a streaming flow on a thin annular disk in the presence of fixed boundaries (Davis 1991b). Hence the model actually treated here is a periodic stack of planes of thin annular disks, with alternate planes perfectly aligned so that each plane containing disks is a plane of symmetry of the flow. The subsequent sections present the detailed analysis to determine array permeability for the most general periodic array allowed by the symmetry restriction. Then calculations are carried out for particular arrays.

2. FORMULATION OF THE PERMEABILITY PROBLEM

A mean flow, $-U\hat{\mathbf{x}}_3$, is disturbed by the presence of a three-dimensional periodic array of thin, rigid annular disks, in broadside position to the flow. The surfaces of the disks are given by

$$\mathbf{r} = \mathbf{r}_n + t(\cos\psi\ \hat{\mathbf{x}}_1 + \sin\psi\ \hat{\mathbf{x}}_2), \quad (1-\epsilon \leqslant t \leqslant 1+\epsilon,\ -\pi < \psi \leqslant \pi), \tag{2}$$

where

$$\mathbf{r}_n = n_1\mathbf{a}^{(1)} + n_2\mathbf{a}^{(2)} + n_3\mathbf{a}^{(3)} \quad (-\infty < \text{integers } n_1, n_2, n_3 < \infty). \tag{3}$$

Both $\mathbf{a}^{(1)}$ and $\mathbf{a}^{(2)}$ are in the plane of a disk, with $\mathbf{a}^{(1)} = d_1\hat{\mathbf{x}}_1$, and with $\mathbf{a}^{(3)}$ denoting the separation and lateral displacement between two disks in adjacent planes. The Reynolds number of the

viscous, incompressible flow is assumed to be sufficiently small for the velocity field $\mathbf{v}$ to satisfy the creeping flow equations

$$\mu\nabla^2\mathbf{v} = \text{grad}\, p \qquad [4]$$

$$\text{div}\, \mathbf{v} = 0 \qquad [5]$$

where μ is the viscosity and p the dynamic pressure. The no-slip boundary condition requires that $\mathbf{v} = \mathbf{0}$ for all $\mathbf{r}$ defined by [2].

To simplify the calculation, the disks are arranged such that each one lies in a plane of symmetry of the flow. This is accomplished by perfect alignment of alternate planar arrays and then by aligning the remaining planar arrays or by offsetting them by a half distance. Hence $\mathbf{a}^{(3)} = D\hat{\mathbf{x}}_3 + v_1\mathbf{a}^{(1)} + v_2\mathbf{a}^{(2)}$, where D is the distance between adjacent planes, and (v_1, v_2) may have the values (0,0), (0,1/2), (1/2,0) or (1/2,1/2), corresponding to perfect alignment, non-alignment in one direction, non-alignment in the other direction, or complete non-alignment.

The symmetry of flow about each disk allows the total disturbance flow to be constructed by distributing normally-directed force singularities over the disks. The pressure jump across a disk provides the density function, and will denoted by

$$\frac{U}{\pi^2}X(t,\psi) = \frac{U}{\pi^2}\left\{X_0(t) + 2\sum_{n=1}^{\infty}[X_{2n}(t)\cos 2n\psi + Y_{2n}(t)\sin 2n\psi]\right\}$$

$$(1-\epsilon \leqslant t \leqslant 1+\epsilon,\ -\pi < \psi \leqslant \pi) \qquad [6]$$

since the given array evidently has period π. If $\mathbf{a}^{(1)}\cdot\mathbf{a}^{(2)} = 0$, the sine terms can be eliminated by choosing $\mathbf{a}^{(j)} = d_j\hat{\mathbf{x}}_j (j = 1, 2)$. The velocity field $\mathbf{V}$, due to force singularities of strength $8\pi\mu\hat{\mathbf{x}}_3$ at the points $\mathbf{r}_n$ (defined by [3]), is now introduced. According to appendix 1, $\mathbf{V}$ can be expressed as

$$\mathbf{V}(\mathbf{r}) = \frac{1}{r}\hat{\mathbf{x}}_3 - x_3\,\text{grad}\left(\frac{1}{r}\right) + \mathbf{V}^{(R)}(\mathbf{r}) \qquad [7]$$

where $\mathbf{V}^{(R)}$ satisfies [4] and [5] everywhere and is given by

$$\mathbf{V}^{(R)}(\mathbf{r}) = -\frac{2\alpha}{\tau}\hat{\mathbf{x}}_3 - (\hat{\mathbf{x}}_3 - x_3\,\text{grad})\left\{\frac{1}{r}\,\text{erf}\left[r\left(\frac{\pi}{\alpha}\right)^{1/2}\right]\right\}$$

$$+ \sum_{\mathbf{n}\neq\mathbf{0}}{}' [\hat{\mathbf{x}}_3 - (x_3 - \mathbf{x}_{n3})\text{grad}]\left\{\frac{1}{|\mathbf{r}-\mathbf{r}_n|}\,\text{erfc}\left[|\mathbf{r}-\mathbf{r}_n|\left(\frac{\pi}{\alpha}\right)^{1/2}\right]\right\}$$

$$+ \frac{8\pi}{\tau}\sum_{\mathbf{K}\neq\mathbf{0}}{}' \frac{1}{K^2}\left[\hat{\mathbf{x}}_3 - \left(\frac{\alpha}{4\pi} + \frac{1}{K^2}\right)K_3(K_1\hat{\mathbf{x}}_1 + K_2\hat{\mathbf{x}}_2 + K_3\hat{\mathbf{x}}_3)\right]e^{i\mathbf{K}\cdot\mathbf{r} - \alpha K^2/4\pi}, \qquad [8]$$

where α is a "moderate constant" (Hasimoto 1959) and $\tau = \mathbf{a}^{(1)}\cdot(\mathbf{a}^{(2)}\times\mathbf{a}^{(3)})$. Hence, from [6] and [7], the total flow field can be written

$$\mathbf{v} = -U\hat{\mathbf{x}}_3 + \frac{U}{\pi^2}\int_{-\pi}^{\pi}\int_{1-\epsilon}^{1+\epsilon} X(t,\psi)\{(\hat{\mathbf{x}}_3 - x_3\,\text{grad})[(x_1 - t\cos\psi)^2 + (x_2 - t\sin\psi)^2 + x_3^2]^{-1/2}$$

$$+ \mathbf{V}^{(R)}[\mathbf{r} - t(\cos\psi\,\mathbf{x}_1 + \sin\psi\,\mathbf{x}_2)]\}t\,dt\,d\psi. \qquad [9]$$

The symmetry has already eliminated tangential flow at each disk, and no normal flow is ensured by satisfying the integral equation

$$\frac{1}{\pi^2}\int_{1-\epsilon}^{1+\epsilon}\left\{X_0(t)G_0(\rho,t) + 2\sum_{n=1}^{\infty}[X_{2n}(t)\cos 2n\theta + Y_{2n}(t)\sin 2n\theta]G_{2n}(\rho,t)\right\}t\,dt$$

$$= 1 - \frac{1}{\pi^2}\int_{-\pi}^{\pi}\int_{1-\epsilon}^{1+\epsilon} X(t,\psi)V_3^{(R)}[(\rho\cos\theta - t\cos\psi)\hat{\mathbf{x}}_1 + (\rho\sin\theta - t\sin\psi)\hat{\mathbf{x}}_2]t\,dt\,d\psi,$$

$$(1-\epsilon \leqslant \rho \leqslant 1+\epsilon,\ -\pi < \theta \leqslant \pi), \qquad [10]$$

where

$$G_m(\rho, t) = \int_{-\pi}^{\pi} \frac{\cos m\theta \, d\theta}{(\rho^2 + t^2 - 2\rho t \cos\theta)^{1/2}}. \quad [11]$$

In [7], $\mathbf{V}^{(R)}$ evidently plays the role of a reflected velocity field due to the rigid boundaries of other disks.

By integrating the Fourier series [6] for the pressure jump, the force on each disk is found to be

$$-16U\mu \int_{1-\epsilon}^{1+\epsilon} X_0(t)t \, dt \, \hat{\mathbf{x}}_3 = -16U\mu F_0 \hat{\mathbf{x}}_3,$$

after defining

$$F_{2n} = \int_{1-\epsilon}^{1+\epsilon} X_{2n}(t)t \, dt \ (n \geqslant 0), \quad H_{2n} = \int_{1-\epsilon}^{1+\epsilon} Y_{2n}(t)t \, dt \ (n \geqslant 1). \quad [12]$$

The mean pressure gradient due to the array of disks is therefore $16U\mu F_0/\tau$ and must, by Darcy's law, be equated to $U\mu/\kappa$, where the permeability κ is dimensionless because the length scale has been set equal to unity. Hence κ is determined by

$$\kappa = \tau/16F_0. \quad [13]$$

3. ASYMPTOTIC SOLUTION FOR THIN DISKS

It has been demonstrated that a viscous fluid is reluctant to flow through an annular disk (Davis 1991a) or a torus (Stewartson 1983), and consequently the flux factor and force coefficient change slowly as the annular width decreases, i.e. as ϵ decreases. One method for solving an integral equation for flow past an annular disk in the presence of fixed boundaries is an asymptotic technique for $\epsilon \to 0$, which was the technique of Davis (1991b) for flows which are axisymmetric but not necessarily symmetric about the plane of the disk. Fortunately the dimensions of the rings in the present application are suitable for the use of such asymptotics, having identified the role of $V_3^{(R)}$ by its appearance as a reflected velocity field in [10].

It was subsequently realized that Leppington & Levine (1972) had used a superior method for a similar calculation, and their simpler method is adopted here. By use of formulas given by Gradshteyn & Ryzhik (1980), the integral in [11] can be expressed in terms of a toroidal Legendre function, and then a hypergeometric function is available which has an asymptotic expansion for values of the argument close to unity. By this technique,

$$G_m(\rho, t) \sim 2\ln\left[\frac{16\min(\rho^2, t^2)}{|\rho^2 - t^2|}\right] - 4\sum_{s=1}^{m} \frac{1}{2s-1} \text{ for } \rho \simeq t,$$

and, after setting

$$\rho = 1 + \epsilon x, \quad t = 1 + \epsilon y, \quad [14]$$

$$G_m(x, y) \sim 2\ln\left(\frac{8}{\epsilon|x-y|}\right) - 4\sum_{s=1}^{m} \frac{1}{2s-1} \ (-1 \leqslant x \neq y \leqslant 1, \epsilon \ll 1). \quad [15]$$

Then the leading order terms in [10] can be written down by setting $t = 1$ on the right-hand side and substituting [6], [14] and [15] to obtain, on considering Fourier components,

$$2F_0\ln\left(\frac{8}{\epsilon}\right) + 2\int_{-1}^{1} X_0^*(y)\ln\left(\frac{1}{|x-y|}\right)dy = \pi^2 - F_0 f_{00} - 2\sum_{m=1}^{\infty}(F_{2m}f_{0m} + H_{2m}h_{0m})$$

$$2\begin{bmatrix} F_{2n} \\ H_{2n} \end{bmatrix}\left[\ln\left(\frac{8}{\epsilon}\right) - 2\sum_{s=1}^{2n}\frac{1}{2s-1}\right] + 2\int_{-1}^{1}\begin{bmatrix} X_{2n}^*(y) \\ Y_{2n}^*(y) \end{bmatrix}\ln\left(\frac{1}{|x-y|}\right)dy$$

$$= -F_0\begin{bmatrix} f_{n0} \\ h_{0n} \end{bmatrix} - 2\sum_{m=1}^{\infty}\left(F_{2m}\begin{bmatrix} f_{nm} \\ h_{mn} \end{bmatrix} + H_{2m}\begin{bmatrix} h_{nm} \\ g_{nm} \end{bmatrix}\right) \quad (n \geqslant 1) \quad [16]$$

where

$$\begin{bmatrix} f_{nm} \\ g_{nm} \\ h_{nm} \end{bmatrix} = \frac{1}{\pi}\int_0^{\pi}\int_0^{\pi} \begin{bmatrix} \cos 2n\theta \cos 2m\psi \\ \sin 2n\theta \sin 2m\psi \\ \cos 2n\theta \sin 2m\psi \end{bmatrix} \{V_3^{(R)}[(\cos\theta - \cos\psi)\,\hat{\mathbf{x}}_1 + (\sin\theta - \sin\psi)\,\hat{\mathbf{x}}_2]$$

$$+ V_3^{(R)}[(\cos\theta - \cos\psi)\,\hat{\mathbf{x}}_1 + (\sin\theta + \sin\psi)\,\hat{\mathbf{x}}_2]\}\mathrm{d}\theta\,\mathrm{d}\psi \qquad [17]$$

and

$$\begin{bmatrix} X_{2n}^*(y) \\ Y_{2n}^*(y) \end{bmatrix} = \epsilon \begin{bmatrix} X_{2n}(t) \\ Y_{2n}(t) \end{bmatrix}, \quad \text{i.e.} \int_{-1}^{1} \begin{bmatrix} X_{2n}^*(y) \\ Y_{2n}^*(y) \end{bmatrix} \mathrm{d}y \sim \begin{bmatrix} F_{2n} \\ H_{2n} \end{bmatrix}. \qquad [18]$$

Each equation, therefore, reduces to the form

$$\int_{-1}^{1} Z(y) \ln\left(\frac{1}{|x-y|}\right) = \mathrm{d}y = C, \quad (-1 \leqslant x \leqslant 1)$$

whose solution

$$Z(y) = \frac{C}{\pi \ln 2} \frac{1}{\sqrt{1-y^2}} \quad (-1 < y < 1)$$

displays, in the simplest manner, the expected square-root singularities in the pressure jump at the rim. However, after solving [16] for $\{X_{2n}^*(y); n \geqslant 0\}$ and $\{Y_{2n}^*(y); n \geqslant 1\}$, only the integral of $Z(y)$ is required in [18] to obtain the following linear system of equations for the ratios $\{F_{2n}/F_0, H_{2n}/F_0; n \geqslant 1\}$:

$$F_0\left[2\ln\left(\frac{16}{\epsilon}\right) + f_{00}\right] + 2\sum_{m=1}^{\infty}(F_{2m}f_{0m} + H_{2m}h_{0m}) = \pi^2$$

$$2\begin{bmatrix} F_{2n} \\ H_{2n} \end{bmatrix}\left[\ln\left(\frac{16}{\epsilon}\right) - 2\sum_{s=1}^{2n}\frac{1}{2s-1}\right] + F_0\begin{bmatrix} f_{n0} \\ h_{0n} \end{bmatrix} + 2\sum_{m=1}^{\infty}\left(F_{2m}\begin{bmatrix} f_{nm} \\ h_{mn} \end{bmatrix} + H_{2m}\begin{bmatrix} h_{nm} \\ g_{nm} \end{bmatrix}\right) = \begin{bmatrix} 0 \\ 0 \end{bmatrix} \quad (n \geqslant 1). \qquad [19]$$

This system must be truncated, not only for practical purposes but also because of the presence of the psi-function which appears in the asymptotic expansion [15]. The first equation of [19] yields the required π^2/F_0 in terms of the zero-order approximation as well as a series involving the ratios $\{F_{2n}/F_0; H_{2n}/F_0; n \geqslant 1\}$ which are determined by the remaining equations. The coefficients, defined by [17], are found by expanding the normal velocity at an infinitesimally thin disk, due to singularities at all other disks in the periodic array, in a double Fourier series that is evidently symmetric in θ and ψ. The coefficients depend on the geometrical arrangement of the disks, but not on ϵ which does not enter the calculation until [19] is solved. Note that f_{00} signifies the axisymmetric effect on one disk of all other disks and suggests the notion of an "equivalent medium", similar to the medium which arises for a random array of small spheres. The non-axisymmetric terms turn out to be small or negligible in the subsequent computations.

4. CALCULATIONS OF PERMEABILITY FOR PARTICULAR ARRAYS

4.1. Matching a thin annular disk to a torus

Having developed relations to describe flow past thin annular disks, the disks are now equated to tori (rings) so that the development can be applied to arrays of rings. Each torus is considered to have radii a and R as defined in figure 1. When the asymptotic formula for the force coefficient

for an annular disk (Davis 1991a) is equated to that for a torus (Stewartson 1983), it is found that a/R corresponds to $\epsilon e^{1/2}/2$. In the current formulation, the relative width of the annulus is 2ϵ, instead of ϵ as in the work cited above, and consequently the comparison is between $\ln(16/\epsilon)$ and $[\ln(8R/a) + 1/2]$. The reason for this change is to use the mean radius of the annulus as the length scale defined by the disk. Kim & Kim (1991) have recently shown, with higher-order accuracy than is required here, that when the mean radius is used as the length scale, the terms of order ϵ obtained by Leppington & Levine (1972) and Spence (1970) are thereby absorbed and so the relative error in the leading-term asymptotic estimate of the drag is of order ϵ^2. Table 1 demonstrates this accuracy by comparing the drag computed by Davis (1991a) to the asymptotic estimate, based on the mean radius.

It may be shown that the $O(\epsilon^2)$ error estimate remains valid when fixed boundaries are introduced (Davis 1991b), provided that the leading term in the reflected velocity field $\mathbf{V}^{(R)}$ is evaluated at the center-line of all rings, as in [17]. Consequently, the error due to the use of asymptotic estimates in the calculations which follow is within about 1% for values of ϵ less than 0.1. The calculations are therefore carried out for $\epsilon < 0.1$.

4.2. Square arrays

With the disks equated to rings, the theory in section 3 is now applied to arrays of rings. The first application is to the initial array described in section 1.1, the one in which the rings form a square lattice in each plane and are aligned in the flow direction. The side of each square is b, as indicated in figure 1, and B is the distance between planes. Thus, in [3],

$$\mathbf{a}^{(1)} = \frac{b}{R}\hat{\mathbf{x}}_1, \quad \mathbf{a}^{(2)} = \frac{b}{R}\hat{\mathbf{x}}_2, \quad \mathbf{a}^{(3)} = \frac{B}{R}\hat{\mathbf{x}}_3.$$

Hence $\tau = b^2B/R^3$ in [A5] and the solid volume fraction of the medium is given by

$$\phi = 2\pi^2\left(\frac{a}{R}\right)^2\left(\frac{R}{b}\right)^2\frac{R}{B}, \qquad [20]$$

or, $(a/R)^2 = \tau\phi/2\pi^2$.

It follows that the dimensionless combination k/a^2 corresponds exactly to $2\pi^2\kappa/\phi\tau$, where κ is the dimensionless permeability in [13]. This last equation shows that, for this particular ring model, the approximation to the permeability is given by

$$\frac{k}{a^2} \approx \frac{\pi^2}{8\phi F_0}.$$

The symmetry of the square array reduces the period of the velocity field to $\pi/2$, with no sine terms in the density function. A sufficiently accurate solution is obtained by writing

$$X(t, \psi) = X_0(t) + 2X_4(t)\cos 4\psi$$

Table 1. Estimates of drag on an annular disk

Radii ratio $\left(\frac{1-\epsilon}{1+\epsilon}\right)$	ϵ^{-1}	Asymptotic estimate $\pi^2/2(1+\epsilon)\ln\left(\frac{16}{\epsilon}\right)$	Calculation by Davis (1991a)	% Error
1/2	3	0.9561	0.9810	−2.54
2/3	5	0.9385	0.9494	−1.15
4/5	9	0.8937	0.8977	−0.45
5/6	11	0.8749	0.8778	−0.33
8/9	17	0.8314	0.8329	−0.18
11/12	23	0.8006	0.8015	−0.13
24/25	49	0.7257	0.7259	−0.03
49/50	99	0.6631	0.6634	−0.05
99/100	199	0.6088	0.6094	−0.11

in [6], whence [19] reduces to

$$F_0\left[2\ln\left(\frac{16}{\epsilon}\right)+f_{00}\right]+2F_4f_{02}=\pi^2$$

$$2F_4\left[\ln\left(\frac{16}{\epsilon}\right)-\frac{352}{105}\right]+F_0f_{20}+2F_4f_{22}=0.$$

The simplest three-dimensional array is the cubical lattice, i.e. $B=b$. This array may be thought of in terms of the cell model, in which each ring is at the centre of a cubical cell of side b. Permeabilities were calculated for this array, and there are various ways to present the results because there are several independent variables. Perhaps the way to start is to fix the cell size b relative to the ring radius a, and vary the ring size R. With b/a fixed, varying R/a means that the solid volume fraction ϕ also varies. Results are given first for $b/a=100$, which corresponds to solidities of order 10^{-4}, i.e. to a very dilute system. This order is appropriate for macromolecular filters, as noted earlier, and is at the low end of the range of ϕ in the present work.

The upper end of the range is dictated by several conditions. The first is to meet the slender-body restriction, $\epsilon<0.1$, which is found to correspond to a maximum value of 0.08 for a/R. The second condition is that one ring must be effectively in the far field of other rings, that is, there must be adequate spacing between adjacent rings in the same plane. The closest distance is taken to be five ring radii, and so the restriction on b is $b>2R+5a$. The third restriction is on B, and its minimum value is taken to be $10a$ to create far-field conditions between rings in adjacent planes. When these restrictions are combined, the maximum value for ϕ is 0.03, which is within the practical range for filters.

Calculated permeabilities are presented in figure 2 for the cubical array, and for the equivalent "offset" array, i.e. the array which is identical except that alternate planes are shifted $b/2$ in each lateral direction as described in section 1.1. Despite the shift, every plane in the offset array remains a plane of symmetry of the flow, so that the use of stokeslets only remains valid, with

$$\mathbf{a}^{(1)}=\frac{b}{R}\hat{\mathbf{x}}_1,\quad \mathbf{a}^{(2)}=\frac{b}{R}\hat{\mathbf{x}}_2,\quad \mathbf{a}^{(3)}=\frac{B}{R}\hat{\mathbf{x}}_3+\frac{b}{2R}(\hat{\mathbf{x}}_1+\mathbf{x}_2).$$

Figure 2 shows that the permeability for this offset array is below that for the cubical array, as expected, but it is only just below, indicating that the more tortuous flow paths have little effect on flow resistance in this dilute regime. The range of R/a in the figure is dictated by the conditions given in the prior paragraph: R/a must be greater than 12.1 to satisfy $\epsilon<0.1$, and R/a must be less than 95/2 to satisfy $b>2R+5a$ and $b/a=100$.

As the ring size and therefore the solidity increase in figure 2, the permeability naturally decreases. However, once the rings nearly fill the cubical cells and R/a approaches 50, the permeability is seen to increase again and hence minima are created. The two minima are indistinguishable and are found to correspond to the ring size which causes maximum blockage within a plane. More specifically, it is the size which makes the area inside the rings equal to the area outside. As mentioned earlier, Stewartson (1983) showed that fluid is reluctant to flow through a ring, and equating areas removes this reluctance. This condition is met when $b/R=\sqrt{2\pi}$, and when $b/a=100$ as in the present case, the corresponding value of R/a is $100/\sqrt{2\pi}$ or about 40. The minima are close to this value in the figure.

The assumption is made in the prior paragraph that the flux through a ring is equal to the flux around the ring if the corresponding areas are equal. This principal is not unreasonable, but its exactness needs to be established because use is made of the principle throughout the discussion of results. The principle, hereafter referred to as the equal-area principle, is dealt with in appendix 2 where the flux through a ring is calculated. The work there shows that, for the geometrical conditions of interest, the flux through a ring is close to the flux if no rings were present, the difference being comparable with other small neglected terms. This calculation is equivalent to comparing fluxes inside and outside a ring. Hence the equal-area principle holds to order ϵ.

The system can be made more concentrated by making the rings thicker or by bringing the planes closer together, and then differences between the aligned and offset arrays are expected.

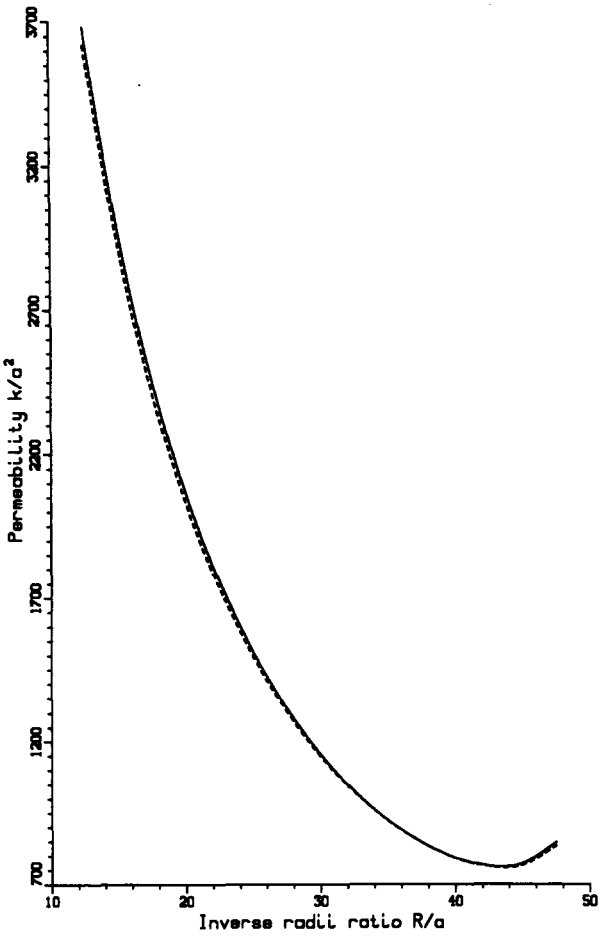

Figure 2. The permeability of two periodic arrays of rings, each comprised of the planes in figure 1 with $b/a = 100 = B/a$. The solid curve is for an array in which the ring centers form a cubical lattice. The dashed curve is for an "offset" array, which is the same as the cubical array except that every other plane is offset to create maximum blockage of the flow.

Calculations were carried out for a system in which both changes were made, namely b/a was reduced to 50 and B/a to 20. For this cell size, the range of R/a is 12.1–22.5, and the range of ϕ extends to 0.01, which approaches the maximum of 0.03 permitted by the theory. The calculated permeabilities are shown in figure 3. The offset array is now distinctly below the aligned array—hereafter termed the square array—which illustrates the significance of tortuosity. For the square array, the equal-area principle for minimal permeability should still apply. Indeed, there is a minimum when R/a is about 20.5, which is close to the theoretical value of $(50/\sqrt{2\pi})$. For the offset array, the planes are too closely spaced for the principle to apply and the permeability continues to drop as R/a and the solidity increase.

The two curves nearly coincide at R/a around 19, which is found to be the condition for maximum shielding in the offset case. The geometry for $R/a = 19$ is sketched in figure 4, and it is seen that the center ring is shielded by arcs of the four rings in front of it. For this spacing, shielding is comparable to that when one ring lies behind another. Hence, the difference in permeability between aligned and offset rings ought to be minimal, which is what figure 3 shows at $R/a = 19$.

4.3. The equilateral array

Another arrangement which can be investigated using the general theory is the array formed of planes in which the ring centers are at the vertices of an equilateral triangle, as illustrated

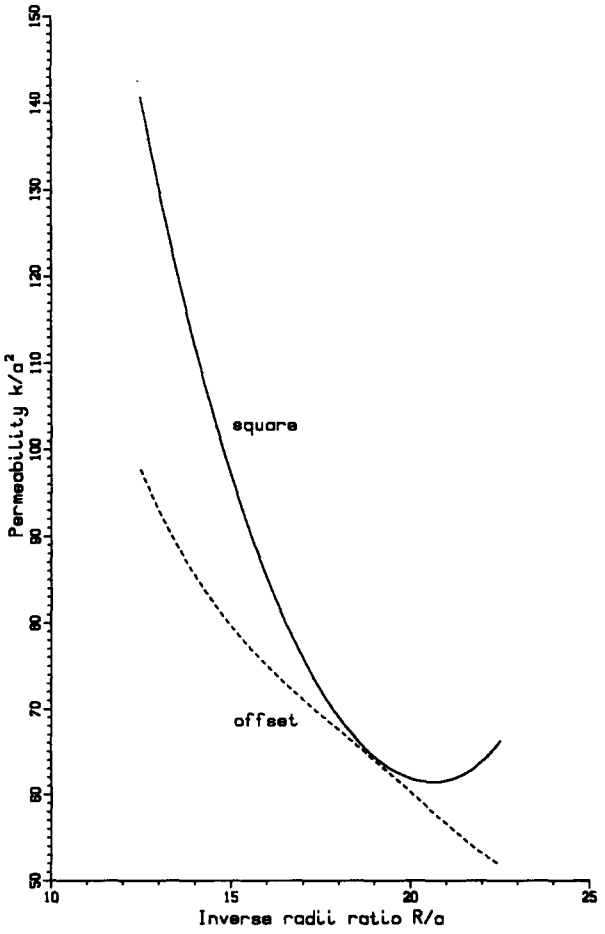

Figure 3. Permeability of aligned and offset arrays of rings. The arrays are similar to those in figure 2 but the rings are larger and the planes are more closely spaced, with $b/a = 50$ and $B/a = 20$.

figure 5. As indicated, the center-to-center distance is still b The rings are taken to be aligned, in which case the vectors of [3] are

$$\mathbf{a}^{(1)} = \frac{b}{R}\hat{\mathbf{x}}_1, \quad \mathbf{a}^{(2)} = \frac{1}{2}\frac{b}{R}(\hat{\mathbf{x}}_1 + \sqrt{3}\hat{\mathbf{x}}_2), \quad \mathbf{a}^{(3)} = \frac{B}{R}\hat{\mathbf{x}}_3.$$

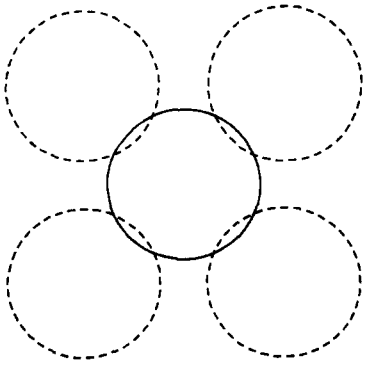

Figure 4. The offset array for $R/a = 19$ and $b/a = 50$, which are the conditions in figure 3 where the permeability curves nearly touch. The dashed rings are in one plane and the solid ring is in the plane behind. Note how this spacing causes the central ring to be well shielded by the four upstream rings.

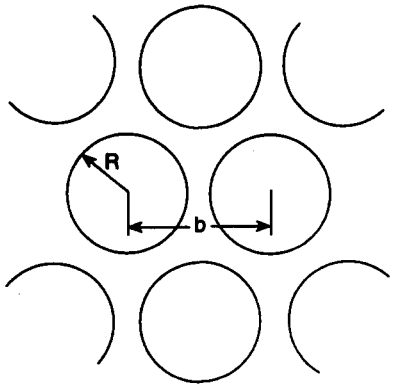

Figure 5. The equilateral array is made up of planes in which the ring centers form equilateral triangles.

Hence $\tau = \sqrt{3}b^2B/2R^3$, and the solid volume fraction and permeability are respectively increased and decreased by the factor $2/\sqrt{3}$ relative to the square array; that is,

$$\phi = \frac{4\pi^2}{\sqrt{3}}\left(\frac{a}{R}\right)^2\left(\frac{R}{b}\right)^2\frac{R}{B}. \qquad [21]$$

Thus again,

$$\frac{k}{a^2} \approx \frac{\pi^2}{8\phi F_0}.$$

The velocity field now has period $\pi/3$, with no sine terms in the density function. The estimate

$$X(t, \psi) = X_0(t) + 2X_6(t)\cos 6\psi$$

in (6) then reduces [19] to

$$F_0\left[2\ln\left(\frac{16}{\epsilon}\right) + f_{00}\right] + 2F_6 f_{03} = \pi^2$$

$$2F_6\left[2\ln\left(\frac{16}{\epsilon}\right) - \frac{13016}{3465}\right] + F_0 f_{30} + 2F_6 f_{33} = 0.$$

As shown by figure 5, the distribution of solid material in a plane is more uniform for this array than for the square array (figure 1), and consequently the permeability should be lower. This comparison is made in figure 6, for the same ring size and the same solidity, and for completeness the offset array is included. With a/R and ϕ fixed, k/a^2 depends primarily on in-plane spacing and hence k/a^2 is plotted versus b/R. It must be kept in mind that, as b/R increases, B/R decreases to keep ϕ constant, according to [20] and [21].

Plotted in this way, a minimum is again found for each array. For the square and offset arrays, the minima occur when b/R is about 2.40, which is close to the equal-area value of $\sqrt{2\pi}$. When the equal-area principle is applied to the equilateral array, it is found that the condition is $b/R = (4\pi/\sqrt{3})^{1/2}$ or 2.69. The minimum of the equilateral curve in figure 6 is close to this theoretical value.

A number of other features of figure 6 should be noted:

(i) the permeability for the equilateral array is below that for the square array, confirming that the more uniform distribution of ring material causes this medium to be less permeable;

(ii) for the square and equilateral arrays, the permeability rises rapidly with b/R. The aligned rings in these arrays can be thought of as rows of rings in the flow direction. As b/R increases the rows become increasingly isolated, and they become more compact because B/R simultaneously decreases. Hence the flow passages between the rows of rings become larger and the permeability rises;

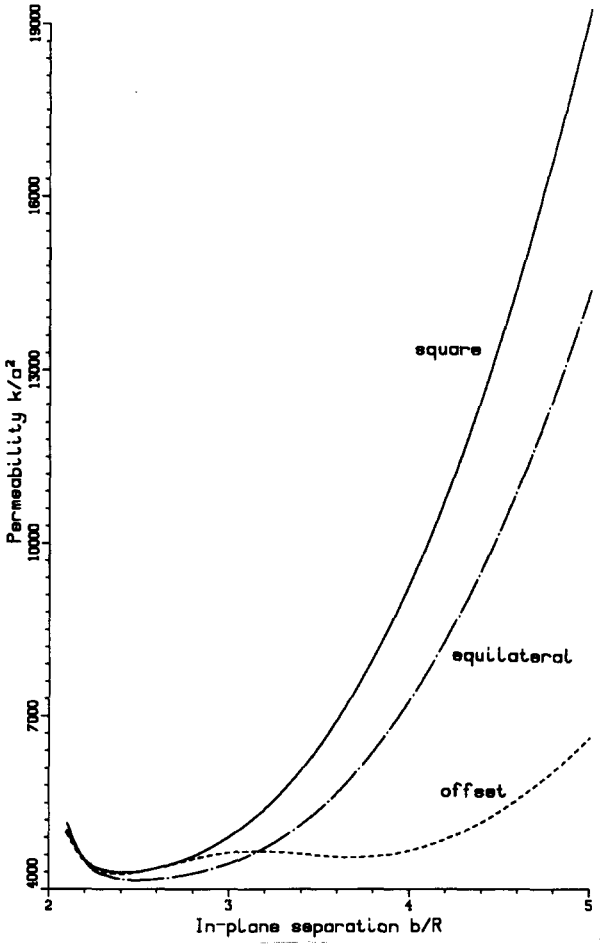

Figure 6. The dependence of permeability on ring spacing within the plane. The ring size $a/R = 0.01$ and the solid volume fraction $\phi = 0.0002$.

(iii) the offset array does not exhibit this same pattern—k/a^2 is virtually constant for b/R up to about 4. The difference is due, of course, to misalignment of the rings. The passages which are clear for the aligned rings are now filled with misaligned rings, and this blockage remains as the rings separate. However, as b/R becomes very large, the offset array also evolves to rows of rings, but the rows are not as compact as those in the comparable square array. Hence k/a^2 should increase when b/R is sufficiently large. Figure 6 indicates that this behaviour starts when b/R exceeds about 4;

(iv) k/a^2 is 6000 for the square array when b/R is about 3.40, and when b/R is about 4.80 for the offset array. The arrays with these spacings are illustrated in figure 7, with the dashed circles in (b) indicating rings in an adjacent plane. In viewing these arrays, it should be kept in mind that B/R is 0.85 in (a) and 0.43 in (b); hence adjacent planes are much closer in the offset array. The two arrays in figure 7 appear to be identical. In fact, the center-to-center distance in (b) is 3.40 (*viz.*, $4.80/\sqrt{2}$), the same distance as in (a). Hence it is not surprising that these are the conditions which produce the same permeability for these two arrays.

The results in figure 6 are for highly dilute systems, and the corresponding curves for more concentrated systems are given in figure 8 where ϕ is 0.01 instead of 0.0002. At first glance, it seems that figure 6 has been repeated with a different ordinate scale, but that is not the case and there is actually a slight difference in the shapes of the two sets of curves. The similarity of figures 6 and 8 is in contrast to the distinct sets of curves for the same two solidities in figures 2 and 3. Because

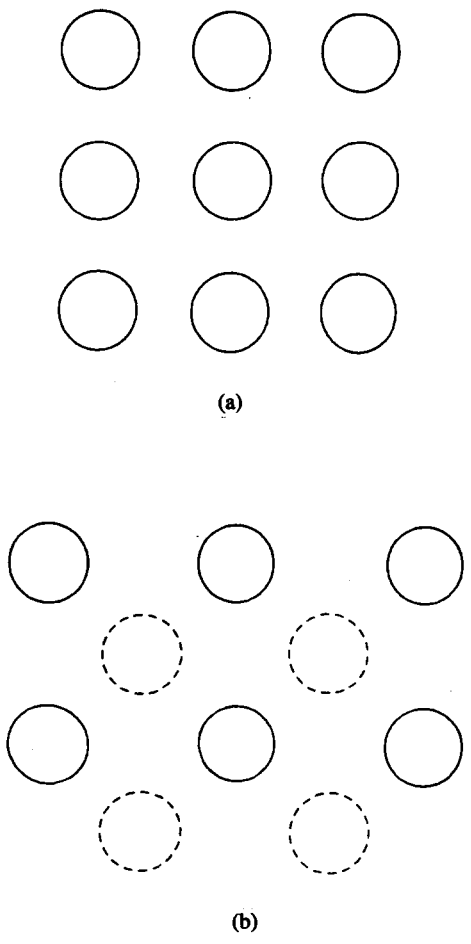

Figure 7. Geometric similarity of two arrays. (a) square array, with $b/R = 3.40$; (b) offset array, with $b/R = 4.80$, and with rings in one plane (solid) shown along with rings in an adjacent plane (dashed); when the two planes are superposed as shown, the center-to-center distance is the same as in (a). Figure 6 shows that the dimensionless permeability is the same for both arrays, namely 6,000.

of the similarity, this way of presenting the results—k/a^2 vs b/R, with a/R and ϕ fixed—is probably the best format for illustrating the permeability characteristics of ring arrays.

We have so far investigated the effects of ring size (figures 2 and 3) and in-plane spacing (figures 6 and 8). The remaining geometrical factor to consider is the spacing between planes. This factor, B/R, is related to shielding and some aspects of shielding have already been made evident. Still it is worthwhile to investigate this factor systematically and so k/a^2 is plotted versus B/R in figure 9. Here the ring size a/R is fixed and the blockage is optimal, i.e. b/R is $\sqrt{2\pi}$ for the square array and $(4\pi/\sqrt{3})^{1/2}$ for the equilateral array. The influence of B/R is much less relevant for the offset array, and so this array is not included. In viewing this figure, it must be kept in mind that as B/R increases ϕ decreases proportionately because a/R and b/R are fixed. For large values of B/R, the flow past one plane does not affect the flow through the next and then flow resistances are linearly additive. The consequence is that k should be linear in B and that is the pattern seen in the figure. Another feature of the plot is the minima. These arise because of shielding at small values of B/R. That is, as B/R decreases and the rings move closer behind one another, each contributes less to the overall resistance and so the permeability rises. The interesting point is that the permeability rises even though the solid volume fraction is increasing.

The prior graphs do not reveal the influence of curvature, which was an objective of this work. Probably the best way of doing so is to compare present permeabilities with those for rod arrays.

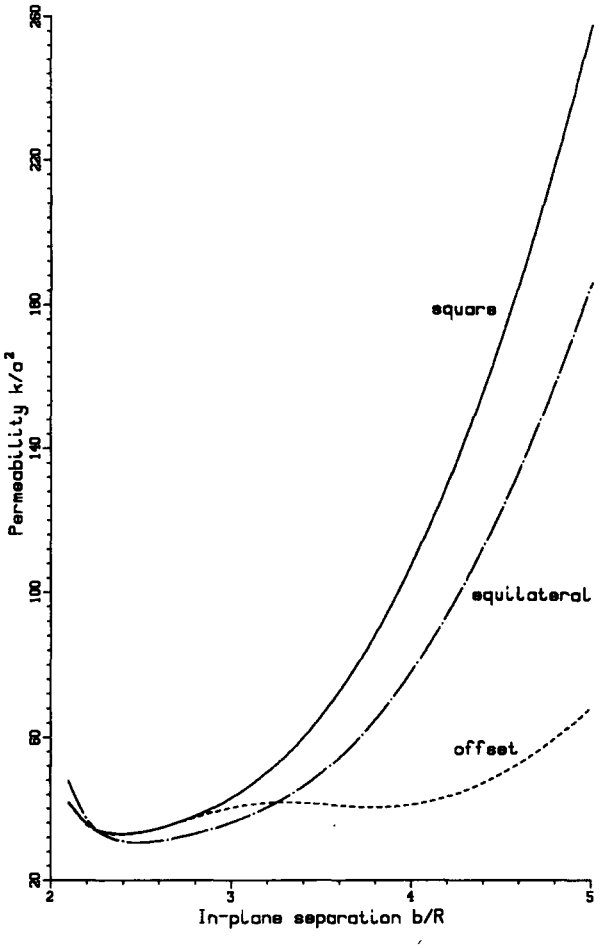

Figure 8. The dependence of permeability on in-plane spacing, with $a/R = 0.08$ and $\phi = 0.01$ for comparison with figure 6. The curves appear to be identical but the permeability scale is different because the rings are eight times thicker and ϕ is 50 times higher.

The dimensionless permeability for the basic rod array (the period square array) is a function of one independent variable only, ϕ, as given in [1]. For ring arrays, however, k/a^2 is a function of three dimensionless parameters—specifically, three of ϕ, a/R, b/R, and B/R. The four are not independent because they are related to each other through [20] or [21]. With more independent variables for ring arrays, it is not immediately obvious how to choose the variables to achieve equivalence of the rod and ring arrays and to facilitate their comparison. One certain basis for comparison is that the solid volume fraction ϕ must be the same, i.e. for the square arrangement of rings,

$$\left(\frac{\pi a^2}{B^2}\right)_{\text{rods}} = \left(\frac{2\pi^2 a^2 R}{Bb^2}\right)_{\text{rings}}, \qquad [22]$$

where B for the rod array is the spacing between rods. B is then the distance between planes for both arrays, and this spacing must be the same because any comparison of ks is fundamentally a comparison of pressure gradients in the flow direction, and thus material must be distributed equally in this direction. Another evident basis for making a comparison is that the rod radius must be equal to the ring radius. With a and B the same, the preceding relation simplifies to

$$\left(\frac{2\pi RB}{b^2}\right)_{\text{rings}} = 1. \qquad [23]$$

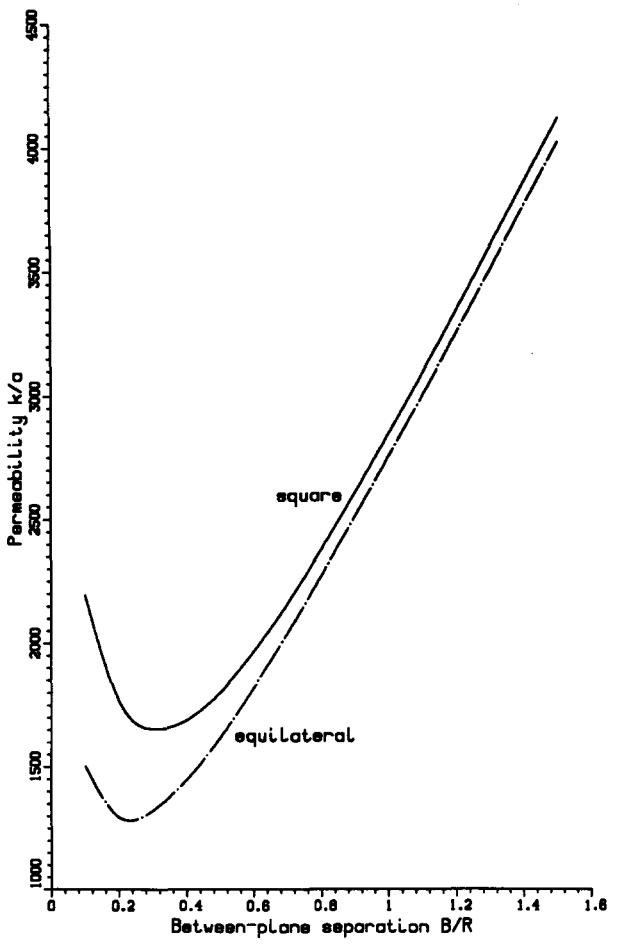

Figure 9. The dependence of permeability on between-plane spacing. The ring size $a/R = 0.01$ and the in-plane spacing $b/R = \sqrt{2\pi}$ or $(4\pi/\sqrt{3})^{1/2}$ for the square or equilateral array respectively. Thus ϕ is proportional to R/B, according to [20], [21].

Various combinations of b/R and B/R will satisfy [23] and an obvious choice is the one which makes ring spacing in a plane as uniform as possible. In a rod array, the spaces between solid elements are uniform throughout; in a ring array, the spaces cannot be uniform, and one way of making them as uniform as possible is to invoke the equal-area principle, i.e. to make $b/R = \sqrt{2\pi}$. It then follows from [23] that B/R is equal to unity.

The permeability of a square ring array was calculated for the above conditions, and the ratio of this permeability to that for a rod array at the same ϕ was found and plotted in figure 10. The analogous ratio was found for the equilateral array (where R is again found to be equal to B) and this ratio is also given in figure 10. The plot clearly demonstrates that these ring arrays are more permeable than equivalent rod arrays. The ratios tend to unity as the solidity decreases, which is expected because the effect of curvature diminishes as ϕ (i.e. a/R) goes to zero. As ϕ increases, the ratios increase but never become very large. For solidities up to 0.01, the difference in permeability between ring and rod arrays is no more than 15%.

Other combinations for b/R and B/R which satisfy [23] are possible, and the effect of offset planes could also be investigated. These combinations will not be explored in a systematic way here, but results from one particular combination will illustrate that there are exceptions to the general result of figure 10. This particular case is the one for which the ring diameter is equal to the plane spacing, i.e. $R = B/2$, and hence $b/R = 2\sqrt{\pi}$. When these conditions are applied to the square array, it is found that the permeability is uniformly about 2% less than that for the condition in figure 10.

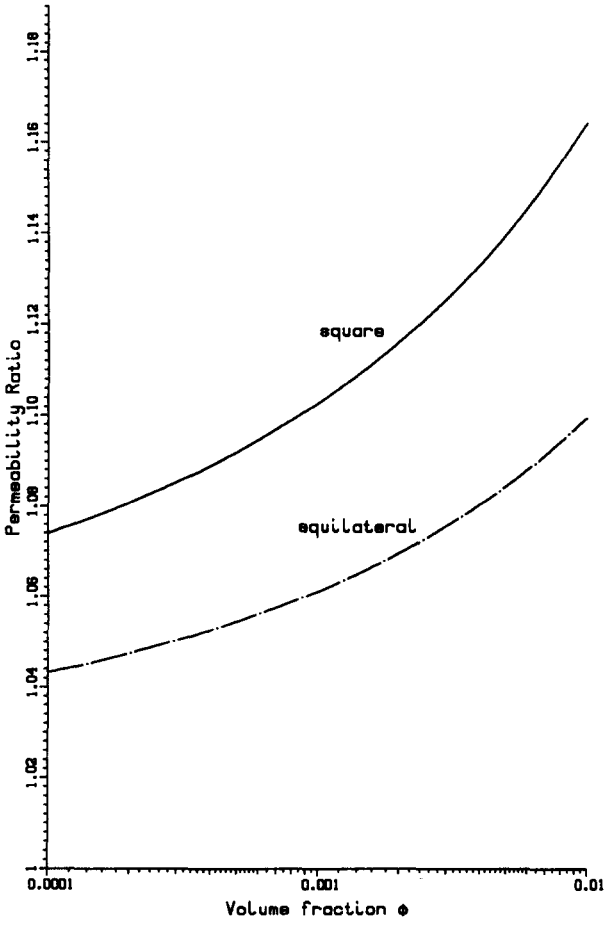

Figure 10. Relative permeability. The ordinate is the ratio of the permeability of a ring array to that for the equivalent rod array. The in-plane spacings are identical to those in figure 9 and the between-plane spacing is in each case the same as the ring radius ($B/R = 1$).

And when the conditions are applied to the offset array, calculations show that the permeability is less than that of the equivalent rod array. This latter comparison is presented in table 2 where it is seen that the relative permeability is less than unity, in contrast to figure 10. (In the table, ϕ extends only to 0.0016 to satisfy $a/R < 0.08$.) The ratios in table 2 are not much below unity—in fact, the amount below is comparable to the contribution of the neglected terms in the analysis—but they are such as to suggest that a ring array may be less permeable than a rod array.

Table 2. Permeability of an offset ring array relative to an equivalent rod array

ϕ	$\frac{k/a^2(\text{rings})}{k/a^2(\text{rods})}$
1.00×10^{-4}	0.9939
1.59	0.9935
2.51	0.9931
4.00	0.9925
6.31	0.9919
10.00	0.9910
15.85	0.9899

5. CONCLUSION

The primary finding of this work is that an array of rings is generally more permeable than an equivalent rod array. With rods, the solid elements are distributed in the most uniform way possible. With rings, the solid elements are variably oriented and curved, but these factors generally do not compensate for the non-uniform spacing of the elements. However, the tortuosity induced by curvature can, under the right circumstances, compensate for the uneven spacing, as the ratios of close to unity in table 2 demonstrate.

This work has been carried out for dilute systems, for solid volume fractions up to 0.01. For higher solidities curved elements might contribute more resistance than rods, and this trend is apparent in table 2 for non-aligned rings. For aligned rings, however, the trend in figure 10 is the reverse: ring arrays are increasingly more permeable as the solid fraction rises.

The present work is also useful for the purpose of making estimates of the permeability of a filter or of any other fibrous porous medium. The results demonstrate that a rod array is a reasonable model for any homogeneous fibrous medium, and its permeability is a virtual lower bound. That is, as a first approximation, the permeability of a homogeneous fibrous medium is equal to that of the equivalent rod array; to a second approximation, the permeability is of order 10% higher. Hence reliable estimates of permeability for fibrous materials can be made for engineering purposes.

REFERENCES

Battista, O. A. 1964 *Synthetic Fibers in Paper Making*. Interscience Publishers, John Wiley & Sons, New York.

Bolam, F. 1962 *The Formation and Structure of Paper*, Vol. 2. The British Paper and Brand Makers Association, figure 8(b), p. 854.

Cox, R. G. 1970 The motion of long slender bodies in a viscous fluid, part 1. General theory. *J. Fluid Mech.* **44,** 791–810.

Davis, A. M. J. 1991a Slow viscous flow due to motion of an annular disk; pressure driven extrusion through an annular hole in a wall. *J. Fluid Mech.* **231,** 51–71.

Davis, A. M. J. 1991b Stokes drag on a narrow annular disk sedimenting in the presence of fixed boundaries or other disks. *Phys. Fluids* **A3,** 249–257.

Drummond, J. E. & Tehir, M. I. 1984 Laminar viscous flow through regular arrays of parallel solid cylinders. *Int. J. Multiphase Flow* **10,** 515–540.

Evald, P. P. 1921 Die Berechnung optischer und elektrostatischer Gitterpotentiale. *Ann. Phys.* **64,** 253–287.

Gradshteyn, I. S. & Ryzhik, I. M. 1980 *Tables of Integrals, Series and Products* (enlarged edition, Edited by A. Jeffrey). Academic Press, New York.

Hasimoto, H. 1959 On the periodic fundamental solutions of the Stokes equations and their application to viscous flow past a cubic array of spheres. *J. Fluid Mech.* **5,** 317.

Howells, I. D. 1974 Drag due to the motion of a Newtonian fluid through a sparse random array of small fixed rigid objects. *J. Fluid Mech.* **64,** 449–475.

Isenberg, I. H. 1967 *Pulp and Paper Microscopy*, 3rd Edition. Institute of Paper Chemistry, figure 100A.

Jackson, G. W. & James, D. F. 1986 The permeability of fibrous porous media. *Can. J. Chem. Eng.* **64,** 364–374.

Johnson, R. E. & Wu, T. Y. 1979 Hydrodynamics of low-Reynolds-number flow, Part 5. Motion of a slender torus. *J. Fluid Mech.* **95,** 263–277.

Kim, M.-V. & Kim, J.-U. 1991a Stokes drag on a circular annulus. *J. Phys. Soc. Japan* **60,** 3679–3691.

Kirsch, A. A. & Fuchs, N. A. 1967 Studies on fibrous aerosol filters—II: Pressure drops in systems of parallel cylinders. *Ann. Occup. Hyg.* **10,** 23–30.

Leppington, F. G. & Levine, H. 1972 Some axially symmetric potential problems. *Proc. Edin. Math. Soc.* **18,** 55–76.

Lighthill, M. J. 1976 Flagellar hydrodynamics. *SIAM Review* **18,** 161–230.

Ogston, A. G., Preston, B. N. & Wells, J. D. 1973 On the transport of compact particles through solutions of chain polymers. *Proc. Royal Soc.* **A333,** 297–316.
Sangani, A. S. & Acrivos, A. 1982 Slow flow past periodic arrays of cylinders with application to heat transfer. *Int. J. Multiphase Flow* **8,** 193–206.
Sangani, A. S. & Yao, C. 1988 Transport processes in random arrays in cylinders II, Viscous flow. *Phys. Fluids* **31,** 2435–2444.
Spence, D. A. 1970 A Wiener–Hopf solution to the triple integral equations for the electrified disc in a coplanar gap. *Proc. Camb. Philos. Soc.* **68,** 529–545.
Stewartson, K. 1983 Mass flux through a torus in Stokes flow. *Z. Angew. Math. Phys.* **34,** 567–574.
Yu, C. P. & Soong, T. T. 1975 A random cell model for pressure drop prediction in fibrous filters. *J. Appl. Mech., Trans. ASME* **22,** 301–304.

APPENDIX 1

Perodic Array of Force Singularities

The velocity and pressure fields due to a periodic array of force singularities were constructed and rearranged according to the technique of Hasimoto (1959), with some adaptation as described below.

The velocity $\mathbf{V}$ and pressure P due to a force singularity of strength $8\pi\mu\hat{\mathbf{x}}_3$ at $\mathbf{r}=\mathbf{z}$ can be expressed as

$$\mathbf{V}=\Phi\hat{\mathbf{x}}_3-(x_3-z_3)\text{grad}\,\Phi,\quad P=-2\mu\frac{\partial\Phi}{\partial x_3}, \tag{A1}$$

where the harmonic function Φ is given by

$$\Phi=\frac{1}{2\pi^2}\int\int\int\frac{1}{k^2}e^{i\mathbf{k}\cdot(\mathbf{r}-\mathbf{z})}d\mathbf{k}=|\mathbf{r}-\mathbf{z}|^{-1}$$

after axisymmetric inversion in (k_1,k_2,k_3) space. However, for a periodic array of such singularities at $\mathbf{r}_n$, defined by [3], it is necessary to write [A1] as

$$\mathbf{V}=\frac{1}{\pi^2}\int\int\int\frac{1}{k^2}\left(\hat{\mathbf{x}}_3-\frac{k_3\mathbf{k}}{k^2}\right)e^{-i\mathbf{k}\cdot(\mathbf{r}-\mathbf{z})}\,d\mathbf{k},\qquad P=\frac{\mu}{\pi^2}\int\int\int\frac{k_3}{ik^2}e^{-i\mathbf{k}\cdot(\mathbf{r}-\mathbf{z})}\,d\mathbf{k} \tag{A2}$$

so that the factor $e^{-i\mathbf{k}\cdot\mathbf{z}}$ in [A2] can be replaced by

$$\sum_{n_1}\sum_{n_2}\sum_{n_3}e^{-i\mathbf{k}\cdot\mathbf{r}_n}=8\pi^3\mathring{\delta}(\mathbf{k}\cdot\mathbf{a}^{(1)})\mathring{\delta}(\mathbf{k}\cdot\mathbf{a}^{(2)})\mathring{\delta}(\mathbf{k}\cdot\mathbf{a}^{(3)}),$$

where $\mathring{\delta}$ denotes the periodic delta function defined by

$$\mathring{\delta}(\theta)=\sum_{l=-\infty}^{\infty}\delta(\theta-2l\pi)=\frac{1}{2\pi}\sum_{-\infty}^{\infty}e^{-in\theta}.$$

The values $\mathbf{K}_m$ of $\mathbf{k}$ at which contributions to the Fourier integral arise are then determined by integral multiples of $(2\pi)^{-1}\mathbf{k}\cdot\mathbf{a}^{(j)}(j=1,2,3)$, i.e.

$$\mathbf{K}_m=2\pi(m_1\mathbf{b}^{(1)}+m_2\mathbf{b}^{(2)}+m_3\mathbf{b}^{(3)}), \tag{A3}$$

where

$$\mathbf{b}^{(1)}=\frac{1}{\tau}(\mathbf{a}^{(2)}\times\mathbf{a}^{(3)}),\quad \mathbf{b}^{(2)}=\frac{1}{\tau}(\mathbf{a}^{(3)}\times\mathbf{a}^{(1)}),\quad \mathbf{b}^{(3)}=\frac{1}{\tau}(\mathbf{a}^{(1)}\times\mathbf{a}^{(2)}), \tag{A4}$$

and

$$\tau=\mathbf{a}^{(1)}\cdot(\mathbf{a}^{(2)}\times\mathbf{a}^{(3)}) \tag{A5}$$

denotes the volume of each "cell". Hence the expressions [A2] now yield

$$\mathbf{V}=\frac{8\pi}{\tau}{\sum_{\mathbf{K}\neq\mathbf{0}}}'\frac{1}{K^2}\left[\hat{\mathbf{x}}_3-\frac{K_3}{K^2}(K_1\hat{\mathbf{x}}_1+K_2\hat{\mathbf{x}}_2+K_3\hat{\mathbf{x}}_3)e^{i\mathbf{K}\cdot\mathbf{r}}\right]$$

$$\text{grad}\,P=\frac{8\pi\mu}{\tau}\left[\hat{\mathbf{x}}_3+{\sum_{K\neq0}}'\frac{K_3}{K^2}(K_1\hat{\mathbf{x}}_1+K_2\hat{\mathbf{x}}_2+K_3\hat{\mathbf{x}}_3)e^{i\mathbf{K}\cdot\mathbf{r}}\right], \tag{A6}$$

where the summation is over all integral triads (m_1, m_2, m_3) in [A3], except (0,0,0) for which the corresponding contribution is a uniform pressure gradient due to the finite force in each "cell". This is demonstrated by integrating the equation

$$\mu\nabla^2\mathbf{V} = \text{grad}\, P - 8\pi\mu\,\hat{\mathbf{x}}_3 \sum_{\mathbf{n}} \delta(\mathbf{r} - \mathbf{r}_{\mathbf{n}})$$

over a "cell". Note that if the singularities are shifted to $(\mathbf{y} + \mathbf{r}_{\mathbf{n}})$, then factors $e^{-i\mathbf{K}\cdot\mathbf{y}}$ must be inserted in [A6], in which the notation is $\mathbf{K} = K_1\hat{\mathbf{x}}_1 + K_2\hat{\mathbf{x}}_2 + K_3\hat{\mathbf{x}}_3$, $K = |\mathbf{K}|$ for each $\mathbf{K}$ defined by a triad $\mathbf{m}$ in [A4].

After noting that [A6] is of the form

$$\mathbf{V} = S_1\hat{\mathbf{x}}_3 + \text{grad}\frac{\partial S_2}{\partial x_3}, \qquad \text{[A7]}$$

where

$$S_i = \frac{8\pi}{\tau}\sum_{\mathbf{K}\neq\mathbf{0}}{}' \frac{1}{K^{2i}} e^{i\mathbf{K}\cdot\mathbf{r}},$$

the convergence of the series can be crucially improved by using Evald's technique (Evald 1921) to transform the functions in [A7] to

$$S_1 = -\frac{2\alpha}{\tau} + \sum_{\mathbf{n}} \frac{2}{|\mathbf{r} - \mathbf{r}_{\mathbf{n}}|}\text{erfc}\left[|\mathbf{r} - \mathbf{r}_{\mathbf{n}}|\left(\frac{\pi}{\alpha}\right)^{1/2}\right] + \frac{8\pi}{\tau}\sum_{\mathbf{K}\neq\mathbf{0}}{}' \frac{1}{K^2} e^{i\mathbf{K}\cdot\mathbf{r} - \alpha K^2/4\pi}$$

$$\frac{\partial S_2}{\partial x_3} = -\sum_{\mathbf{n}} \frac{(x_3 - x_{n3})}{|\mathbf{r} - \mathbf{r}_{\mathbf{n}}|}\text{erfc}\left[|\mathbf{r} - \mathbf{r}_{\mathbf{n}}|\left(\frac{\pi}{\alpha}\right)^{1/2}\right] + \frac{2i\alpha}{\tau}\sum_{\mathbf{K}\neq\mathbf{0}}{}' \frac{K_3}{K^2}\left(1 + \frac{4\pi}{\alpha K^2}\right) e^{i\mathbf{K}\cdot\mathbf{r} - \alpha K^2/4\pi}$$

where α is a moderate constant.

However, $\mathbf{r}_{\mathbf{0}} = 0$, so the contribution of the $\mathbf{n} = \mathbf{0}$ terms to [A7] can be rearranged as

$$\frac{1}{r}\hat{\mathbf{x}}_3 - x_3\,\text{grad}\left(\frac{1}{r}\right) - \frac{1}{r}\hat{\mathbf{x}}_3\,\text{erf}\left[r\left(\frac{\pi}{\alpha}\right)^{1/2}\right] + x_3\,\text{grad}\left\{\frac{1}{r}\,\text{erf}\left[r\left(\frac{\pi}{\alpha}\right)^{1/2}\right]\right\},$$

in which the first two terms are the usual singular terms due to a force singularity at the origin ($\mathbf{z} = \mathbf{0}$ in [A1]) and the remaining terms are regular at $\mathbf{r} = \mathbf{0}$.

APPENDIX 2

Flux Through a Ring

According to [9], in which lengths are dimensionless, the flux Q through a ring is given by

$$Q = \int_{-\pi}^{\pi}\int_{0}^{1-\epsilon} \hat{\mathbf{x}}_3\cdot\mathbf{v}(s\cos\theta, s\sin\theta, 0)s\,ds\,d\theta$$

$$= -U\pi(1-\epsilon)^2 + \frac{U}{\pi^2}\int_{-\pi}^{\pi}\int_{1-\epsilon}^{1+\epsilon} X(t,\psi)t\,dt\,d\psi \int_{-\pi}^{\pi}\int_{0}^{1-\epsilon} \frac{s\,ds\,d\theta}{[s^2 + t^2 - 2st\cos(\theta - \psi)]^{1/2}}$$

$$+ \frac{U}{\pi^2}\int_{-\pi}^{\pi}\int_{1-\epsilon}^{1+\epsilon} X(t,\psi)t\,dt\,d\psi \int_{-\pi}^{\pi}\int_{0}^{1-\epsilon} \hat{\mathbf{x}}_3\cdot\mathbf{V}^{(R)}[(s\cos\theta - t\cos\psi)\hat{\mathbf{x}}_1$$

$$+ (s\sin\theta - t\sin\psi)\hat{\mathbf{x}}_2]s\,ds\,d\theta. \qquad \text{[A8]}$$

The second double integral in the second term is, according to [11]:

$$\int_{0}^{1-\epsilon} G_0(s,t)s\,ds \sim 4$$

and hence the second term in Q is $\sim(8U/\pi)\mathbf{F}_0$, by use of [12]. So the contribution of the first and second terms to the flux Q is

$$\sim -U\pi\left[1-\frac{8}{\pi^2}F_0\right], \qquad \text{[A9]}$$

which, unless the rings are too close, is

$$\sim -U\pi\left[1-\frac{8}{2\ln\left(\frac{16}{\epsilon}\right)+f_\infty}\right].$$

If the other rings are ignored, this expression reduces, in turn, to

$$-U\pi\left[1-\frac{4}{\ln\left(\frac{16}{\epsilon}\right)}\right],$$

as in [2.20] of Davis (1991a).

Consider now the third term in Q, given by [A8]. From [8],

$$\begin{aligned}\hat{\mathbf{x}}_3\cdot\mathbf{V}^{(R)}[(s\cos\theta-t\cos\psi)\hat{\mathbf{x}}_1+(s\sin\theta-t\sin\psi)\hat{\mathbf{x}}_2] &= -\frac{2\alpha}{r}-\frac{1}{r}\operatorname{erf}\left[r\sqrt{\frac{\pi}{\alpha}}\right]\\ &+\sum_{\mathbf{n}\neq\mathbf{0}}{}'\left[1+\mathbf{x}_{\mathbf{n}3}\frac{\partial}{\partial\mathbf{x}_3}\right]\left\{\frac{1}{|\mathbf{r}-\mathbf{r}_\mathbf{n}|}\operatorname{erfc}\left[|\mathbf{r}-\mathbf{r}_\mathbf{n}|\sqrt{\frac{\pi}{\alpha}}\right]\right\}\\ &+\frac{8\pi}{\tau}\sum_{\mathbf{K}\neq\mathbf{0}}{}'\frac{1}{K^2}\left[1-\left(1-\frac{\alpha}{4\pi}+\frac{1}{K^2}\right)K_3^2\right]e^{i\mathbf{K}\cdot\mathbf{r}-\alpha K^2/4\pi}. \qquad \text{[A10]}\end{aligned}$$

The last term in [A10] requires $\alpha>0$ for convergence but

$$\int_{-\pi}^{\pi}\int_0^1 e^{is(K_1\cos\theta-K_2\sin\theta)}s\,ds\,d\theta=2\pi\frac{J_1[\sqrt{K_1^2+K_2^2}]}{\sqrt{K_1^2+K_2^2}},$$

which enables α to be set equal to 0 in the flux integral, thus assigning the error functions the values 1 and 0 respectively. Then two terms vanish in [A10] while another reduces to $-r^{-1}$ and thus its contribution to Q cancels the second term in [A8]. Hence

$$Q\sim -U\pi+\frac{16U}{\tau}\sum_{\mathbf{K}\neq\mathbf{0}}{}'\frac{\sqrt{K_1^2+K_2^2}}{\mathbf{K}^4}J_1[\sqrt{K_1^2+K_2^2}]\int_{-\pi}^{\pi}\int_{1-\epsilon}^{1+\epsilon}X(t,\psi)e^{-it(K_1\cos\psi+K_2\sin\psi)}t\,dt\,d\psi.$$

The force singularity distribution has been found to be essentially axisymmetric, i.e. $X(t,\psi)\simeq X_0(t)$ and hence, with F_0 defined by [12],

$$Q\sim -U\pi+\frac{32U\pi}{\tau}F_0\sum_{\mathbf{K}\neq\mathbf{0}}{}'\frac{\sqrt{K_1^2+K_2^2}}{K^4}J_1[\sqrt{K_1^2+K_2^2}]J_0[\sqrt{K_1^2+K_2^2}], \qquad \text{[A11]}$$

where, for the square array,

$$K_1=\frac{2\pi m_1}{d},\quad K_2=\frac{2\pi m_2}{d},\quad K_3=\frac{2\pi m_3}{D},\quad \tau=d^2D, \qquad \text{[A12]}$$

The triple summation in [A11] can be regarded as a Riemann sum and hence, for d, $D\gg1$, the flux is approximated by

$$-U\pi+\frac{8U}{\pi}F_0\int_{-\infty}^{\infty}\int_0^{\infty}\frac{k}{(k^2+l^2)^2}J_1(k)J_0(k)k\,dk\,dl=-U\pi\left[1-\frac{8}{\pi^2}F_0\right],$$

as in [A9]. So the $\mathbf{V}^{(R)}$ term in [A8] $\to 0$ as d, $D\to\infty$, as expected.

To demonstrate the equal area/equal flux principle, it is sufficient to consider the limit $D \to \infty$, in which case another Riemann sum yields

$$\frac{2\pi}{D} \sum_{m_3=-\infty}^{\infty} \frac{1}{K^4} \to \frac{\pi}{2(K_1^2+K_2^2)^{3/2}} \qquad (K_1^2+K_2^2 \neq 0).$$

Substitution of [A12] and some rearrangement of the double summation in [A11] then shows that

$$\lim_{D\to\infty} Q \sim -U\pi\left\{1-\frac{8F_0}{\pi^2}\sum_{m_1=1}^{\infty}\sum_{m_2=0}^{\infty}\frac{1}{m_1^2+m_2^2}J_1\left[\frac{2\pi}{d}\sqrt{m_1^2+m_2^2}\right]J_0\left[\frac{2\pi}{d}\sqrt{m_1^2+m_2^2}\right]\right\}. \quad [A13]$$

Computed values of the double sum in [A13] show a fractional flux gain of 0.0369 F_0 at $d = 2.42$, which decreases through 0 at $d = b/R \approx 2.62$ to $-0.0333\ F_0$ at $d = 2.80$. These small fractions are comparable with other neglected terms, and so these estimates are sufficient to demonstrate that, when the ring spacing in each plane is such that the area inside the rings equals the area outside, the flux through a ring is nearly equal to its value in the absence of all rings and hence similar to the flux between the rings. This is described as the equal-area principle in the text.